DRUG DELIVERY
2023, VOL. 30, NO. 1, 2171158
https://doi.org/10.1080/10717544.2023.2171158

Taylor & Francis
Taylor & Francis Group

RESEARCH ARTICLE

OPEN ACCESS Check for updates

Novel Pt(IV) prodrug self-assembled nanoparticles with enhanced blood circulation stability and improved antitumor capacity of oxaliplatin for cancer therapy

Yuanlei Fu[a,b,c,†], Ying Kong[b,c,†], Xiangping Li[b,c], Dongfang Cheng[b,c], Yuqian Hou[b,c], Yan Li[b,c], Tongfang Li[b,c], Yani Xiao[b,c], Qiuyan Zhang[b,c] and Rong Rong[b,c]

[a]School of Pharmacy, Key Laboratory of Molecular Pharmacology and Drug Evaluation (Yantai University), Ministry of Education, Collaborative Innovation Center of Advanced Drug Delivery System and Biotech Drugs in Universities of Shandong, Yantai University, Yantai, Shandong, China; [b]Yantai Key Laboratory of Nanomedicine & Advanced Preparations, Yantai Institute of Materia Medica, Yantai, Shandong, China; [c]Shandong Laboratory of Yantai Drug Discovery, Bohai Rim Advanced Research Institute for Drug Discovery, Yantai, Shandong, China

ABSTRACT

Pt(IV) compounds are regarded as prodrugs of active Pt(II) drugs (i.e. cisplatin, carboplatin, and oxaliplatin) and burgeoned as the most ideal candidates to substitute Pt(II) anticancer drugs with severe side effects. Nanoparticle drug delivery systems have been widely introduced to deliver Pt(IV) prodrugs more effectively and safely to tumors, but clinical outcomes were unpredictable owing to limited in vivo pharmacokinetics understanding. Herein, a novel Pt(IV) prodrug of oxaliplatin(OXA) was synthesized and prepared as self-assembled micellar nanoparticles(PEG-OXA NPs). In vitro, PEG-OXA NPs rapidly released biologically active OXA within 5 min in tumor cells while remaining extremely stable in whole blood or plasma. Importantly, the pharmacokinetic results showed that the $AUC_{0-\infty}$, and $t_{1/2}$ values of PEG-OXA NPs were 1994 ± 117 h·μg/mL and 3.28 ± 0.28 h, respectively, which were much higher than that of free OXA solution (2.03 ± 0.55 h·μg/mL and 0.16 ± 0.07 h), indicating the longer drug circulation of PEG-OXA NPs in vivo. The altered pharmacokinetic behavior of PEG-OXA NPs remarkably contributed to improve antitumor efficacy, decrease systemic toxicity and increase tumor growth inhibition compared to free OXA. These findings establish that PEG-OXA NPs have the potential to offer a desirable self-delivery platform of platinum drugs for anticancer therapeutics.

ARTICLE HISTORY
Received 1 December 2022
Revised 16 January 2023
Accepted 16 January 2023

KEYWORDS
Platinum(IV) prodrug; self-assembled nanoparticles; pharmacokinetics; antitumor efficacy; oxaliplatin

1. Introduction

Approximately 50% of all patients with cancer who receive chemotherapy are treated with platinum anticancer drugs—cisplatin, carboplatin and oxaliplatin (OXA) (Kelland, 2007). These platinum drugs are first-line agents in many kinds of tumors (Motzer et al., 1993; Ibrahim et al., 2004), including ovarian, colorectal, cervical, liver and lung cancer, etc. The combination of platinum-based chemotherapy is a research hotspot in the clinic. However, despite the worldwide application of platinum drugs and their clinically advantageous outcomes in oncology, they are hindered by drug resistance (Ho et al., 2016; Song et al., 2019) due to decreased drug uptake, increased efflux, altered cellular metabolism and activated DNA repair. Another obstacle is the Pt-related toxic side-effects, like vomiting, nausea, nephrotoxicity and neurotoxicity (Oun et al., 2018), which is primarily caused by their poor pharmacokinetic properties, necessitating the useof high doses for effectiveness at the tumor tissue. Therefore, extensive efforts have been devoted to develop a novelgeneration of platinum-based anticancer drugs with higher efficacy and lower side effects.

Recently, Pt(IV)-based compounds (Song et al., 2020; Q. Wang et al., 2021; Huang et al., 2022) are considered as the most promising classes of a new generation platinum drugs. Unlike traditional square-planar Pt(II) drugs (i.e. cisplatin, carboplatin, and OXA), which could be rapidly deactivated by human serum albumin in blood, Pt(IV) compounds exhibit stability during the circulation because they possess six-coordinated octahedral geometry with two adjustable axial ligands to reinforce kinetic inertness and promote cellular uptake. Once inside the cancer cells, Pt(IV) are passively reduced to active Pt(II) by the high intracellular concentrations of reducing agents such as glutathione(GSH), ascorbic acid and mercaptans (Gibson, 2016; Kenny et al., 2017; Yao et al., 2019). So Pt(IV) compounds are regarded as prodrugs of toxic Pt(II) species and burgeoned as the most ideal candidates to substitute Pt(II) mitigating systemic toxicities (Johnstone et al., 2016).

CONTACT Qiuyan Zhang qyzhang@yimm.ac.cn; Rong Rong rrong@yimm.ac.cn
Supplemental data for this article can be accessed online at https://doi.org/10.1080/10717544.2023.2171158.
†These authors have contributed equally to this work.

© 2023 The Author(s). Published by Informa UK Limited, trading as Taylor & Francis Group.
This is an Open Access article distributed under the terms of the Creative Commons Attribution-NonCommercial License (http://creativecommons.org/licenses/by-nc/4.0/), which permits unrestricted non-commercial use, distribution, and reproduction in any medium, provided the original work is properly cited.

Nanoparticle drug delivery systems have been widely introduced to increase drug accumulation in tumor site, reduce toxicity and maximize the drug efficacy through the enhanced permeability and retention (EPR) effect (L. Wang et al., 2017).Up to date, many Pt(IV) prodrugs encapsulated in nanosystems particularly via covalently attached have been developed. In advanced preclinical research, these Pt(IV) nanoparticles have shown at least equivalent efficacy as well as reduced systemic toxicity (Ling et al., 2018; Z.G. Wang et al., 2019; Ding et al., 2020; Z.W. Xu et al., 2022) compared to their small molecule counterparts. However, Pt(IV)-based nanoparticles have not yet been approved by the FDA, possibly due to limited experimental data on the in vivo pharmacokinetic (PK) related with pharmacodynamics (PD) of these nanoparticles (He et al., 2019). One of the reasons is the complexed structures of Pt(IV) prodrugs leading to lack of sensitive and specific analytical strategies to simultaneously determine Pt(IV) compound, released active Pt(II) and metabolites in biological samples. For example, if polymer materials were applied to Pt(IV) nanoparticles, the polydispersity of polymer molecular weight makes the accurately quantitative analysis of Pt(IV) nanoparticles in vivo still a challenge. The current analytical methods, such as radioactive labeling, ELISA and inductively coupled plasma mass spectrometry (ICP-MS) cannot reveal the distribution balance and metabolic mechanism of Pt(IV) complex and its active Pt(II) (Rudmann et al., 2013; Khor et al., 2016). Furthermore, Pt(IV) nanoparticle drug delivery in vivo is intrinsically a multi-step procedure, that depends on PK of the nanoparticle carrier, PK of the Pt payload itself and drug release dynamics that may change relying by the in vivo environmental context. Although this multistep process is important for overall therapeutic outcomes, little experimental investigation exists that interprets how this multi-step process carry out in vivo (Miller et al., 2015). So far, the most commonly reports are the determination of total Pt concentration in vivo using ICP-MS after Pt(IV) nanoparticle administration (Xiao et al., 2014; C. Xu et al., 2019; Zhang et al., 2021), which cannot elucidate the behavior mechanism of Pt(IV) nanomaterial itself in vivo at all. This insufficiency of understanding is obviously a bottleneck in the design and development of more effective therapies.

Our previous research (Feng et al., 2018) have reported a novel Pt(IV) prodrug of OXA that was designated as PEG-OXA (***Scheme 1***) here. PEG-OXA owns two long lipid chains and hydrophilic polyethylene glycol (PEG_{2k}) in axial ligands that can self-assemble into micellar nanoparticles in water, termed as PEG-OXA NPs. In this scenario, our goal was to bring some light on the pharmacokinetic mechanism of the Pt(IV) prodrugs nano-structuration, taking PEG-OXA NPs as a representative example. With this purpose the nanoparticles were prepared and characterized first. Its stability under physiologic conditions, as well as the active OXA release in reducing environment was investigated. After that, the pharmacokinetics characterization of PEG-OXA NPs and the released active OXA in rats was analyzed using a novel ultra-performance liquid chromatography-tandem mass spectrometry (UPLC-MS) coupled with collision-induced dissociation in the ionization source (in-source CID). The in vivo antitumor activity and safety of PEG-OXA NPs were also assessed in mice. These obtained results may provide significant reference for the subsequent research and development of Pt(IV) nanoparticle.

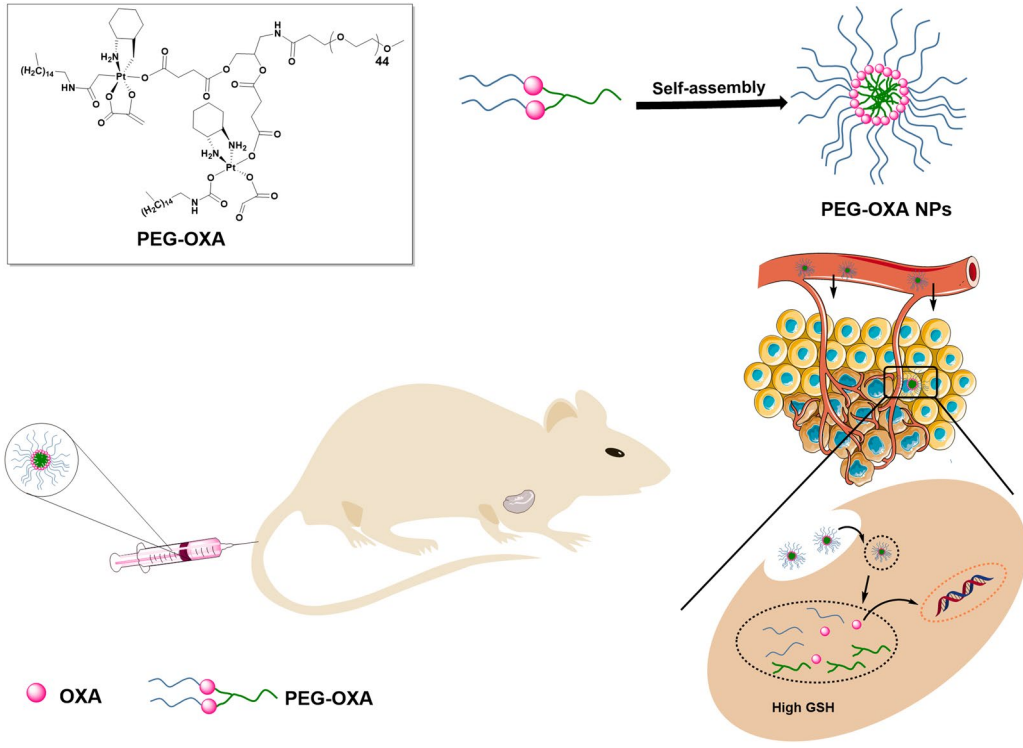

Scheme 1. Strategic illustration of the design and action mechanism of the self-assembled PEG-OXA NPs. PEG-OXA NPs is expected to mitigate side effect of OXA through decreasing free OXA exposure in blood circulation and improve efficacy via prolonging and elevating intratumoral drug exposure.

2. Experimental

2.1. Materials

OXA were supplied by Shandong Boyuan Pharmaceutical Co., Ltd. (Jinan, China). All other reagents used in the synthesis of the PEG-OXA prodrug were purchased from Sigma-Aldrich and used without further purification. Methanol (HPLC grade) was purchased from Fisher Scientific (Pittsburgh, USA). Formic acid (FA) was bought from Fluka Chemie (Buchs, Switzerland). Ultrapure water was prepared from a Milli-Q purification system (Millipore, MA, USA).

HT-29 and SW620 cells were purchased from China infrastructure of cell line resource (Beijing, China) and cultured with dulbecco's modified eagle medium (DMEM) medium (Gibco) added 1% antibiotics and 10% fetal bovine serum (FBS, Gibco).

Sprague-Dawley rats (6–8 weeks old) and ICR mice (4–5 weeks old) were purchased from Pengyue Laboratory Animal Technology Co., Ltd (Jinan, China). Healthy BALb/c nude mice were bought from Gem Pharmatech Co., Ltd, and fed in a specific pathogen-free (SPF) animal laboratory. All the animal experiments reported in this paper were approved by the Committee on the Ethics of Animal Experiments of the Yantai Institute of Materia Medica, and was performed in strict accordance with the guidelines of the National Institutes of Health Guide for the Care and Use of Laboratory Animals.

2.2. Synthesis and characterization of PEG-OXA prodrug

The synthesis of the PEG-OXA prodrug followed previously published work (Feng et al., 2018) and the procedure is shown in Supplementary Scheme S1. OXA-C16 was weighed into a round-bottom flask and dissolved in dichloromethane (DCM). 1-Ethyl-3-(3-dimethylaminopropyl) carbodiimide hydrochloride (EDCI, 3 eq.) was added under nitrogen and reacted at 40 °C for 5 h. Then 4-Pyrrolidinopyridine (4-PPY, 1.5 eq.) and *tert*-butyl *N*-(2,3-dihydroxypropyl) carbamate (0.5 eq.) was added, and the reaction was carried out at 40 °C overnight. After monitored by high-performance liquid chromatography (HPLC), the reaction was extracted twice with ethyl acetate and purified using silica gel column chromatography to obtain the desired product Boc-L-$(OXA\text{-}C16)_2$.

The above product was dissolved in DCM and trifluoroacetic acid (TFA, 1.5 eq.) was added. After stirred at room temperature for 1 h, 2-(7-Azabenzotriazol-1-yl)-N,N,N′,N′-tetramethyluronium hexafluorophosphate (HATU, 2 eq.) and N, N-Diisopropylethylamine (DIPEA,3 eq.) were slowly added. With the mixture dissolved, mPEG2k-COOH was added and the reaction was stirred at room temperature. When the reaction was completed, the organic solvent was removed by rotary evaporation. The purified PEG-OXA was separated by reverse-phase preparative high-performance liquid chromatography (Prep 150, Waters, Milford, USA). PEG-OXA was obtained through lyophilization and stored at 4 °C in powder form prior to use. The successful synthesis of PEG-OXA prodrug was characterized using Electro Spray Ionization-Mass Spectroscopy (ESI-MS) (Supplementary Figure S1), ^{1}H-NMR (Supplementary Figure S2) and ^{13}C-NMR (Supplementary Figure S3), respectively.

2.3. Preparation and characterization of PEG-OXA NPs

Our designed amphipathic prodrug that owns a long lipid chain and hydrophilic polyethylene glycol (PEG2k) in axial ligands can self-assemble into nanomicelles (PEG-OXA NPs) in water. Malvern spray analyzer was used to measure the particle size and size distribution of PEG-OXA NPs. In addition, to observe the morphology of nanomicelles, the PEG-OXA NPs solution was deposited onto a carbon-coated copper grid and stained with 2% phosphotungstic acid. After 2 min, excess solution was removed using filter paper and the copper grid was dried. The PEG-OXA NPs was observed using transmission electron microscopy (TEM, JEM-1400, Tokyo, Japan).

2.4. Critical micelle concentration

The critical micelle concentration of PEG-OXA NPs was measured according to our previous report (Lang et al., 2021) using Nile red as fluorescence probe. Briefly, Phosphate Buffered Saline (PBS) solution of PEG-OXA prodrug in different concentrations was added to the vials containing dried Nile red and sonicated for 40 min and deposited for 4 h. The fluorescence spectrum of Nile red excited at 543 nm and emissive at 660 nm was collected at room temperature using multifunctional enzyme marker (SpectraMax M2e, Sunnyvale, CA). The critical micelle concentration was finally calculated at the inflection point of the plot of fluorescence intensity versus PEG-OXA micelles concentration.

2.5. Cytotoxicity and intracellular drug release of PEG-OXA NPs

The cytotoxicity of PEG-OXA-NPs was assessed by the standard -(4,5-dimethyl-2- thiazolyl)-2,5-diphenyl-2-H-tetrazolium bromide) (MTT) assay as previously reported (X.H. Wang et al., 2020; Lang et al., 2021). HT-29 cells were transferred into a 96-well plate and cultured in DMEM medium with 10% FBS and maintained in a humidified atmosphere of 5% CO_2 at 37 °C for 24 h. Then, the OXA and PEG-OXA NPs solution with different concentrations (0.69–500 μM) were added into the 96-well plate and incubated for 24, and 48 h, respectively. The cytotoxicity of PEG-OXA NPs was evaluated by the MTT cell proliferation assay. To investigate whether the endogenous reducing agent glutathione could effectively reduce the dimeric OXA(IV) prodrug released from nanoparticles to active OXA, HT-29 cells were seeded into 6-well plates (1×10^6 cells/well) and incubated at 37 °C for 24 h prior to study. After the cells attach to the wall, the cell culture media was removed and PEG-OXA NPs (20 μM) diluted with fresh culture medium was added into each well. At predetermined time points (0.083, 0.25, 0.5, 1, 2, 4, 6, 8 and 24 h), the cells and culture medium were collected. The cells were sonicated and centrifuged,

and the concentration of free OXA in the supernatant was analyzed by UPLC-MS/MS system (TSQ Quantiva, Thermo Fisher Scientific, USA) equipped with a Thermo Hypersil GOLD™ column (50 mm × 2.1 mm, 1.9 μm). The column was eluted with a mix of mobile phase consisted of (A) 0.1% (vol/vol) formic acid in water and (B) methanol (A:B, 97:3). The transitions *m*/z 398.1 → 306.0 of OXA was monitored and quantified according to a published report (Ito et al., 2012).

2.6. Blood and plasma stability in vitro

The blood or plasma stability of PEG-OXA prodrug was assessed by monitoring the concentration of PEG-OXA in fresh rat blood or plasma in vitro according to the previous reports. Briefly, 200 μL of PEG-OXA nano-micelles solution (0.5 μg/mL and 25 μg/mL) was incubated with 2 mL of fresh rat blood or plasma at 37 °C. Briefly, 200 μL of the mixture was collected at 0, 30, 60, 90, 120 and 240 min. The blood samples were centrifuged at 12,000 r/min for 5 min to obtain plasma. About 50 μL of plasma sample was mixed with 200 μL of methanol to precipitate protein. After centrifuged at 12,000 r/min for 10 min, UPLC-MS/MS method coupled with collision-induced dissociation in the ionization source (in-source CID) was applied to measure the concentration of PEG-OXA in the supernatant at the scheduled time ($n = 3$ for each group).

The in-source CID spectra of PEG-OXA was generated with a Thermo Fisher TSQ Quantiva triple quadrupole mass spectrometer equipped with an electrospray ionization (ESI) interface and Ultimate 3000 UPLC system (Thermo Fisher Scientific, USA). Chromatographic separation was carried out on a Thermo Hypersil GOLD™ column (50 mm × 2.1 mm, 1.9 μm) and the column oven was maintained at 40 °C. The mobile phase consisted of (A) 0.1% (vol/vol) formic acid in water and (B) methanol using the following gradient elution: 0–1.0 min, 45%B; 1.0–2.0 min, 45–96%B; 2.0–7.0, 96%B; 7.0–7.5 min, 96–45%B; 7.5–8.5 min, 45%B. The flow rate was 0.3 mL/min and the injection volume was 2 μL. The mass spectrometer was operated in positive-ion mode using multiple reaction monitoring (MRM) to monitor the mass transitions. The ionization voltage was set at 3500 V and the source temperature was 350 °C. The sheath gas (N_2) and auxiliary gas were set at 40 and 15 Arb, respectively. The fragmentor voltage value in the ionization source was 80 V. The transitions of PEG-OXA was monitored at *m*/*z* 396.05 →306.0.

2.7. Pharmacokinetic studies

For the pharmacokinetic study, 12 Sprague–Dawley rats (half male, half female) were weighed and divided randomly into two groups: the PEG-OXA NPs group and OXA solution group. Rats in the former group were intravenously administered a single dose of PEG-OXA micelles (equivalent to 5 mg/kg of OXA). Those in the latter group were intravenously administered 5 mg/kg of OXA powered prepared in 5% glucose solution. Blood samples from the rats were collected by retro-orbital puncture at 0.083, 0.25, 0.5, 1, 2, 4, 6, 8, 12 and 24 h after the injection and subsequently centrifuged at 12,000 rpm for 5 min. The resulting plasma layer from the PEG-OXA NPs group was divided into three sections and treated separately to determine the concentration of PEG-OXA and OXA (quantified by UPLC-MS/MS described in sections 2.5 and 2.6) and total Pt. The plasma obtained from the OXA solution group was treated separately to determine the concentration of OXA and total Pt. The Pt content was measured by inductively coupled plasma mass spectrometry (ICP-MS, Icap RQ, Thermo Scientific, USA). The non-compartmental model analysis was used to calculate the pharmacokinetic parameters using Phoenix WinNonlin 7.0 (Pharsight, Mountain View, CA), including area under the concentration-time curve (AUC, expressed as h μg/mL), maximum plasma concentration(C_{max}, μg/mL), the terminal elimination half-life($t_{1/2}$, h), mean residence time (MRT, h) and total clearance (CL, mL/h/kg).

2.8. Toxicity evaluation after repeated dosing

The toxicity study was assessed on the healthy ICR mice (17–18 g, male). The mice were randomly divided into six groups ($n = 10$) and injected one of the following treatments: 5% glucose solution group as the control, free OXA group (7.5 mg/kg), free OXA group (10 mg/kg), PEG-OXA NPs group (7.5 mg/kg in OXA), PEG-OXA NPs group (10 mg/kg in OXA) or PEG-OXA NPs group(15 mg/kg in OXA). The mice were intravenously administrated every 3 days for five times. At the end of the experiment, the major organs were harvested and calculated viscera index. Whole blood was collected for blood routine examination including: white blood cell count (WBC), neutrophils (NE), lymphocyte (LY), red blood cell count (RBC), hemoglobin (HGB), platelet count (PLT) and hematocrit (HCT). Blood was collected and centrifuged to obtain serum for monitoring total protein (TP), albumin (ALB), urea (UREA) and serum creatinine (Cr).

2.9. In vivo antitumor efficacy

BALB/c nude mice (18–20 g, male) were inoculated with SW620 cells (3×10^6 cells) at the third fat pad on the right. When the tumors size reached about 100–200 mm^3, the mice were randomly assigned into six groups, receiving 5% glucose solution group as control group, free OXA group (5 mg/kg, i.v.), free OXA group (10 mg/kg, i.v.), PEG-OXA NPs group (5 mg/kg in OXA, i.v.), PEG-OXA NPs group (10 mg/kg in OXA, i.v.) or PEG-OXA NPs group (20 mg/kg in OXA, i.v.). The mice were dosed once a week for 4 weeks by tail vein injection and the volume of tumor and body weights were measured three times a week. The tumor volume (TV) was calculated from the long diameter (*L*) and short diameter (*W*) of the tumors [TV = ($L \times W \times W$)/2]. Relative tumor volume (RTV) was assessed as V/V_0 (V_0 was the corresponding tumor volume when the treatment was initiated). After tumor monitoring, mice were euthanized and tumors were collected and weighed.

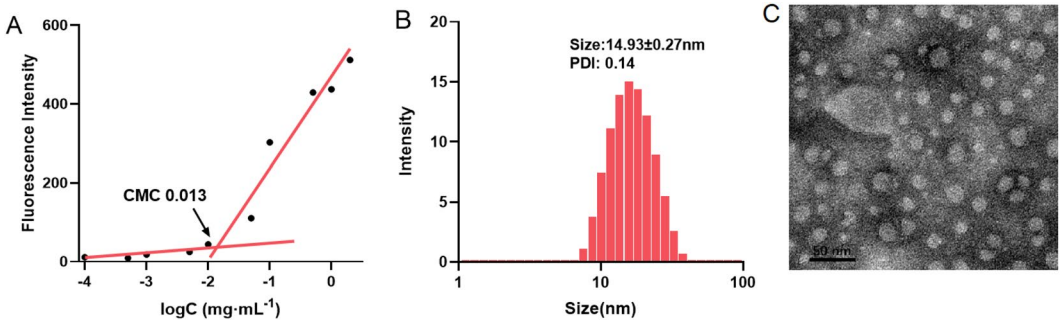

Figure 1. Characterization of PEG-OXA nanoparticles. (A) Critical micelle concentration of PEG-OXA NPs. (B) The hydrodynamic size of PEG-OXA NPs determined by dynamic light scattering. (C) A representative TEM image of PEG-OXA NPs.

2.10. Statistical analysis

The data were conducted in triplicates at least and expressed as means ± standard deviation (SD) and analyzed using Student's *t* test. For a confidence interval of 95%, a value of $p < .05$ was indicative of significant.

3. Results and discussion

3.1. Synthesis and characterization of PEG-OXA NPs

PEG-OXA prodrug was synthesized according to the procedures from previous reports (Supplementary Scheme S1). After modification by polyethylene glycol, the molecular weight of PEG-OXA was normally distributed. The MS signal was analyzed by liquid chromatography-mass spectrometry (LC-MS, 6100, Agilent, USA). By analyzing the molecular weight difference between the clusters of mass spectral signals, found that the mass spectral signals have multiple charges (Supplementary Figure S1). After deconvolution calculations, the molecular weight range is consistent with the target compound. And ^{1}H NMR and ^{13}C NMR confirmed the successful synthesis of the complexes (Supplementary Figures S2 and S3).

PEG-OXA has an amphiphilic prodrug structure that can spontaneously self-assemble into micelles in water. The particle size of the PEG-OXA NPs exhibited spherical morphology in electron microscope and uniform size distribution, with a hydrodynamic diameter of 14.93 ± 0.27 nm and negative surface charge of −0.267 ± 0.025 mV and the OXA theoretical loading efficiency was 21.85%. The two-carbon chain configuration in the prodrug structure can form a stable hydrophobic core, making the micellar system more stable, which can be used for drug administration without excipients. The critical micelle concentration (CMC) determined by Nile Red is ~0.013 mg/mL (***Figure 1***(A–C)).

3.2. Cytotoxicity and intracellular drug release of PEG-OXA NPs

We evaluated the cytotoxicity of PEG-OXA NPs in HT-29 cells by MTT assay. As shown in ***Figure 2***(A), PEG-OXA NPs showed the highest cytotoxicity with an IC_{50} of 7.552×10^{-6} M at 24 h and 6.120×10^{-6} M at 48 h, which was 2.7-fold and 1.7-fold lower than OXA. To exert the desired efficacy, prodrug should be converted to its parental drug. The reduction property of Pt(IV) prodrugs has been deeply explored in recent years. Our previous publication had also demonstrated that

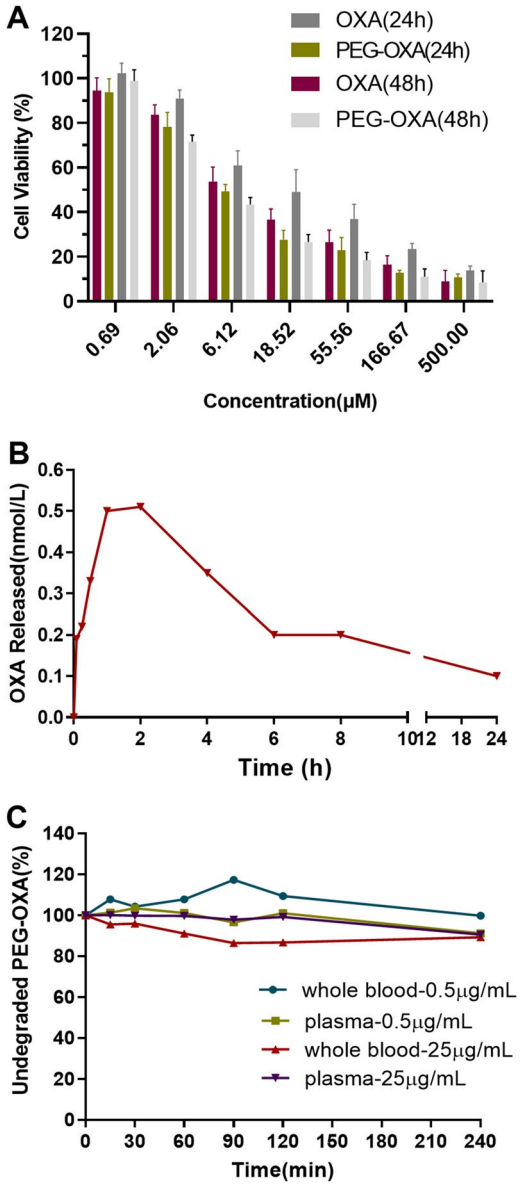

Figure 2. Cell viability, release activity and stability of PEG-OXA nanoparticle. (A) The cell viability rate of OXA and PEG-OXA NPs. (B) The release profile of OXA in HT-29 cells incubated with PEG-OXA NPs. (C) Blood and plasma stability of PEG-OXA NPs in vitro.

PEG-OXA prodrug could be efficiently converted to OXA in a PBS buffer (pH = 7.4) containing equivalents (10 mM) of GSH incubated at 37 °C after 24 h (Feng et al., 2018). Herein, we further evaluated the OXA release from PEG-OXA after incubation with HT-29 cells for 24 h. The release potentials of the OXA is shown in Figure 2(B). OXA could be immediately released from PEG-OXA after 5 min incubation in HT-29 cells and the highest concentration was reached at 4 h with 201.9 nmol/L. It was expected that this reduction-sensitive prodrug micelles could release the drug into active Pt(II) form by the high intracellular concentrations of reducing agents such as GSH once internalized into tumor cells.

3.3. Blood and plasma stability in vitro

Plasma stability is important for Pt(IV) prodrugs. If these compounds could be rapidly degraded by hydrolytic enzymes or inactivating/reducing agents in plasma, they will not have enough concentration at the therapeutic target to be converted to Pt(II) for pharmacological activity and not reduce system toxicity. Instability of plasma can also make the analysis of samples complicated in pharmacokinetic studies. Because the concentration of Pt(IV) prodrugs cannot be measured accurately if compounds continue to decompose after the blood samples collected or during storage. This will lead to erroneous pharmacokinetic data. Therefore, in our study, we investigated the whole blood and plasma stability of PEG-OXA prodrug and summarized the results in Figure 2(C). Compared with the concentration of PEG-OXA (0.5 μg/mL) at 0 min, approximately 99.8% and 91.0% PEG-OXA in whole blood and plasma could be detected at 4 h point, respectively. PEG-OXA content at the high concentration (25 μg/mL) also did not change significantly during 4-h incubation in whole blood and plasma. Contrariwise, no OXA was detectable in this experiment. It was expected that PEG-OXA NPs could protect against hydrolysis or reduction and will be stable in systemic circulation.

3.4. Pharmacokinetics study

Compared with the numerous pharmacological reports, few studies were corelated with the pharmacokinetics of Pt(IV) prodrug. Many only determined the concentration of Pt in rat blood using ICP-MS after injected of Pt(IV) nanoparticles.

Table 1. Summary of the plasma pharmacokinetic parameters in rats following intravenous administration of PEG-OXA NPs or OXA solution (5mg/kg in OXA).

	PEG-OXA NPs		OXA solution	PEG-OXA NPs	OXA solution
Parameters	PEG-OXA	OXA	OXA	Pt	Pt
$T_{1/2}$ (h)	3.28 ± 0.28	5.91 ± 1.45	0.16 ± 0.07	5.96 ± 0.50	17.52 ± 0.52
C_{max} (μg/mL)	581 ± 35.4	0.13 ± 0.02	9.58 ± 1.42	67.12 ± 6.94	4.76 ± 0.68
$AUC_{0\text{-}t}$ (h μg/mL)	1,994 ± 117	0.90 ± 0.23	1.94 ± 0.39	303.6 ± 8.13	13.00 ± 3.44
$AUC_{0\text{-}\infty}$ (h μg/mL)	2,003 ± 119	1.14 ± 0.33	2.03 ± 0.55	314.3 ± 10.0	19.98 ± 5.65
Vz (mL/kg)	53.1 ± 6.26	38.1 ± 6.73	567 ± 70	67.05 ± 3.45	3,220 ± 818
CL (mL/h/kg)	11.2 ± 0.72	4.62 ± 1.06	2,580 ± 560	7.82 ± 0.26	127.98 ± 36.2

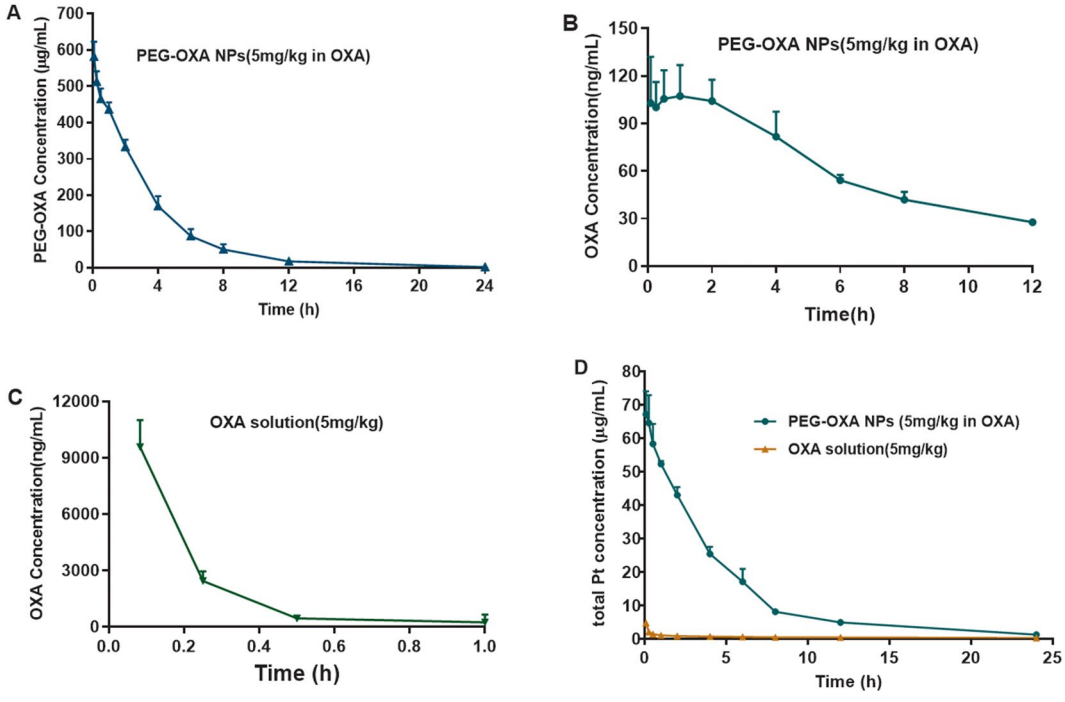

Figure 3. The mean plasma concentration-time curves of PEG-OXA NPs and OXA solution (mean ± SD, $n = 6$). (A) Mean plasma concentration–time curves of PEG-OXA prodrug after intravenous administration of PEG-OXA NPs to rats. (B) Mean plasma concentration–time curves of OXA in rats after intravenous administration of PEG-OXA NPs. (C) Mean plasma concentration–time curves of OXA after intravenous administration of OXA solution to rats. (D) Mean plasma concentration–time curves of total Pt after intravenous administration of PEG-OXA NPs or OXA solution to rats.

However, elucidating the pharmacokinetic behavior of Pt(IV) NPs and its released active Pt(II) but not the total Pt is the most effective method for predicting and interpreting the efficacy and toxicity of Pt(IV) nanoparticle drug delivery system in preclinical and clinical trials. To investigate the pharmacokinetic property of PEG-OXA and whether OXA can be released from PEG-OXA in vivo, we injected PEG-OXA micelles into SD rats through the tail vein at a dose of 22.4 mg/kg (equivalent to 5 mg/kg of OXA). The blood samples were collected at predetermined time points and used to determine the presence of OXA and PEG-OXA in plasma by UPLC-MS analysis. Animals treated with 5 mg/kg of OXA were used to compare the pharmacokinetics of this agents. Results showed that OXA was detected in OXA-treated animals, while both OXA and PEG-OXA were detected in the blood samples of animals administered to PEG-OXA micelles. The corresponding pharmacokinetic parameters calculated using non-compartmental analysis are listed as mean ± SD and presented in ***Table 1***. ***Figure 3***(A,B) shows the mean plasma concentrations of PEG-OXA prodrug and its active Pt(II)-OXA after intravenous administration of PEG-OXA micelles respectively. Figure 3(C) describes the mean plasma concentrations of OXA after intravenous administration of OXA solution. The pharmacokinetic results of PEG-OXA prodrug showed that the $AUC_{0-\infty}$, CL and $t_{1/2}$ values were 1994 ± 117 h·μg/mL, 11.2 ± 0.72 mL/h/kg and 3.28 ± 0.28 h, respectively. The C_{max} value of OXA in PEG-OXA NPs (0.13 ± 0.02 μg/mL) was significantly lower than that obtained with OXA solution (9.58 ± 1.42 μg/mL). The $t_{1/2}$ of OXA in PEG-OXA NPs (5.91 ± 1.45 h) was increased remarkably compared with that of OXA solution (0.16 ± 0.07 h), suggesting that OXA in PEG-OXA NPs was slowly cleared from plasma despite the low initial plasma concentration. The CL of OXA in PEG-OXA NPs (4.62 ± 1.06 mL/h/kg) was also significantly lower than that of OXA solution (2580 ± 560 mL/h/kg). While the $AUC_{0-\infty}$ of OXA in PEG-OXA NPs (1.14 ± 0.33 h·μg/mL) was slightly decreased compared with that of OXA solution (2.03 ± 0.55 h·μg/mL). In addition, compared with the pharmacokinetic behavior of total platinum in plasma after injection of OXA solution in rats, the $AUC_{0-\infty}$ of total Pt (314.3 ± 10.0 h·μg/mL) in PEG-OXA NPs was remarkably increased and the CL of total Pt (7.82 ± 0.26 mL/h/kg) in PEG-OXA NPs was reduced (Table 1 and Figure 3(D)). These results indicated that PEG-OXA NPs could significantly prolong the circulation time and reduce the exposure concentration of OXA in blood, which might be beneficial to increase the interaction time for PEG-OXA NPs releasing OXA in tumor cell, and then achieve better antitumor efficacy and lower toxicity. Our findings demonstrated that PEGylated Pt(IV) nanoparticles could increase blood circulation in vivo and

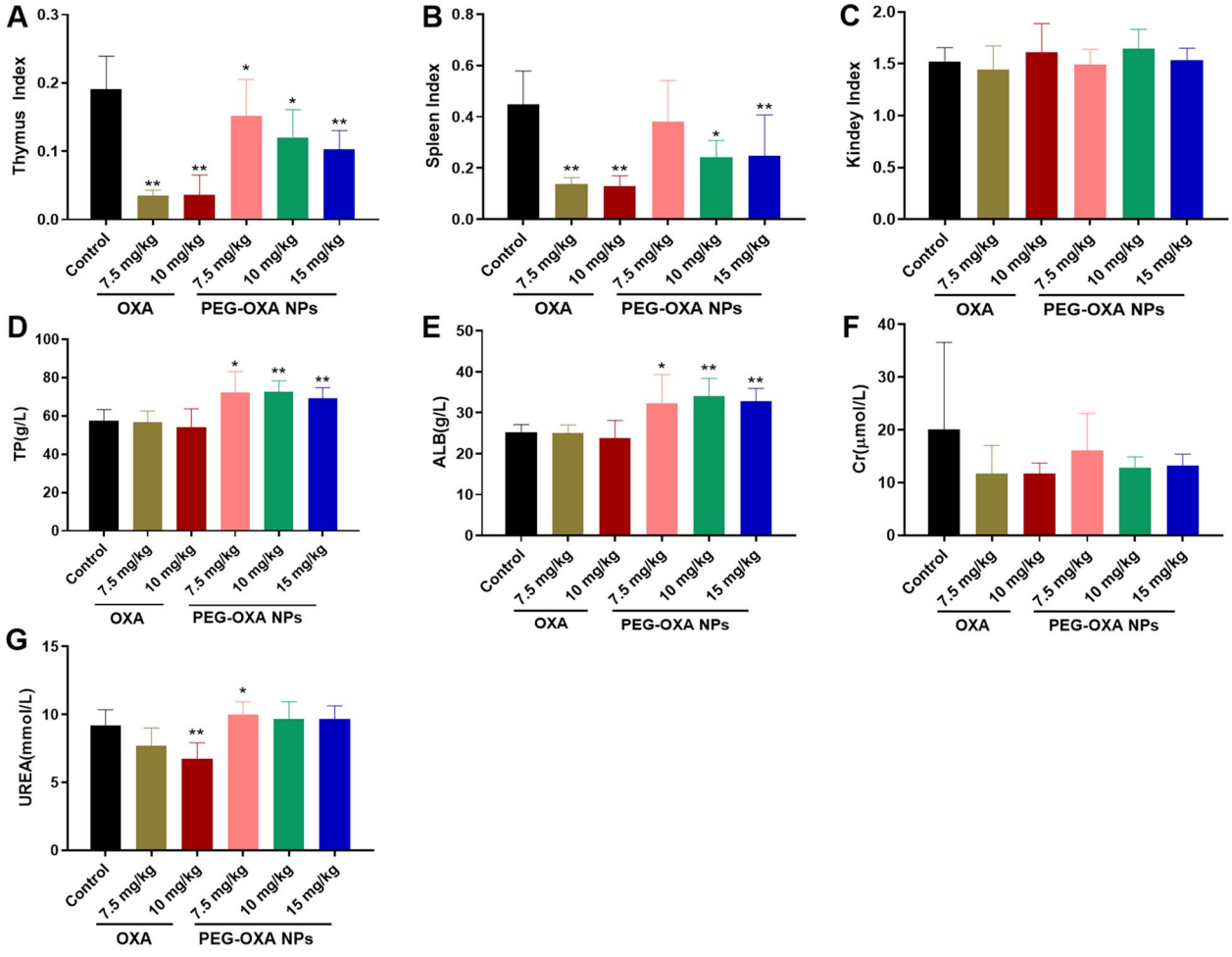

Figure 4. In vivo toxicity evaluation. The viscera index of mice receiving different treatments: (A) thymus, (B) spleen, (C) kidney. Activity changes of (D)TP, (E) ALB, (F) Cr and (G) UREA. All data were presented as mean ± SD. *$p < .05$, **$p < .01$.

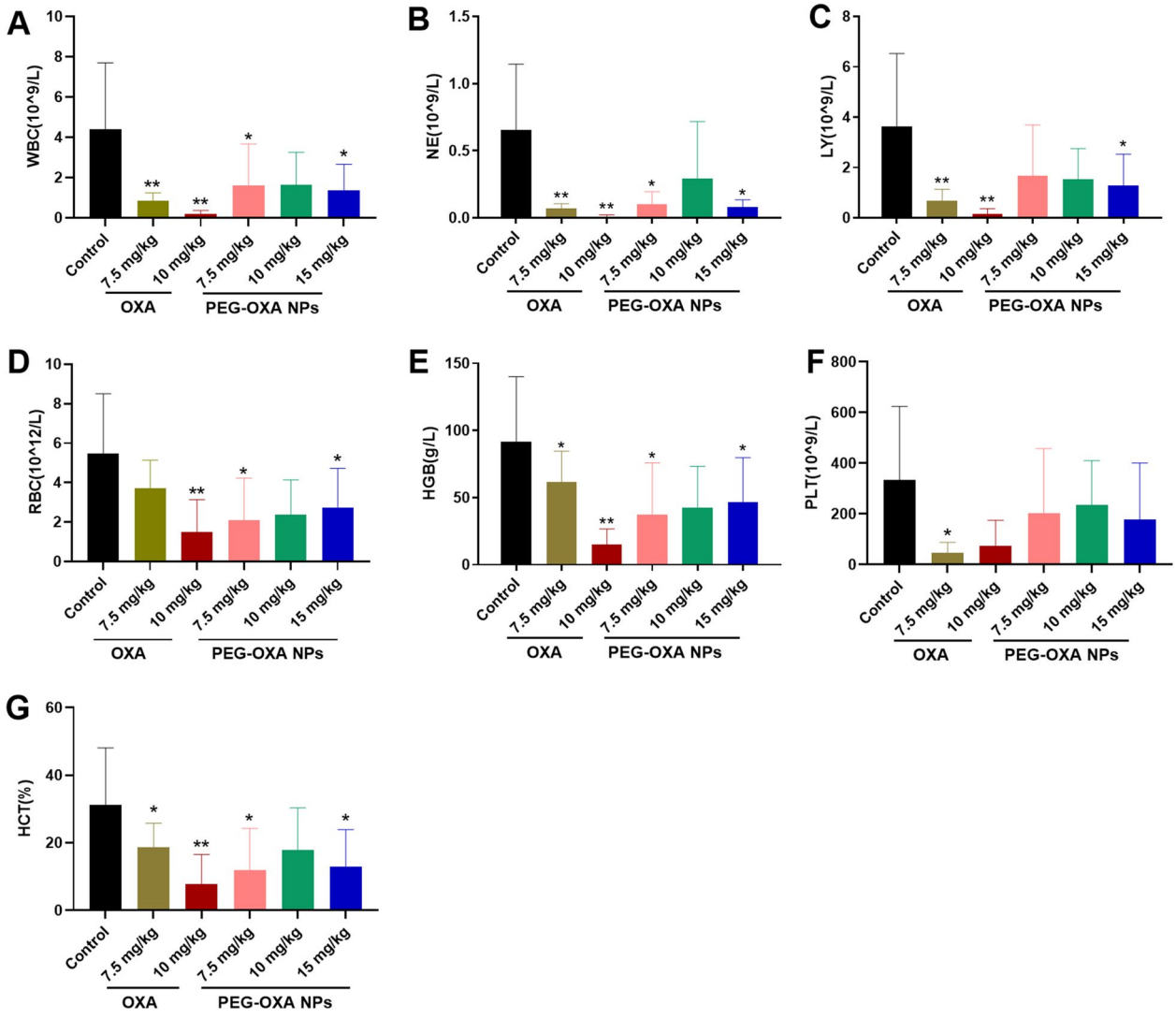

Figure 5. In vivo toxicity evaluation. The blood routine examination of (A) WBC, (B) NE, (C) LY, (D) RBC, (E) HGB, (F) PLT and (G) HCT. All data were presented as mean ± SD. $^{*}p < .05$, $^{**}p < .01$.

avoid elimination by immune cells, which was consistent with previous reports (Pasut & Veronese 2009). As we discussed earlier, PEG-OXA prodrug was stable in blood circulation system and could release the active OXA by reducing agents such as GSH once internalized into tumor cells. We speculated that the low concentration of OXA in plasma after administration of PEG-OXA NPs to rats might be produced by some tissue cells (such as liver) with relatively high concentrations of reducing agents. Meanwhile, we wondered whether the prolonged retention time of PEG-OXA NPs would contribute to better antitumor effect in vivo and the release of OXA in normal tissues would cause side effects, so our further investigation focused on the toxicity and antitumor activity of PEG-OXA NPs.

3.5. In vivo toxicity evaluation

We evaluated the in vivo safety of the PEG-OXA NPs. The thymus index and spleen index of PEG-OXA NPs groups decreased significantly compared with those of control group, indicating that PEG-OXA NPs had certain immunotoxicity, but a significant increase in the thymus and spleen weight were observed in mice receiving PEG-OXA NPs than those receiving OXA, suggesting that PEG-OXA NPs could reduce the immunotoxicity caused by OXA (***Figure 4***(A,B)). Further results also confirmed that all indexes of blood routine test in PEG-OXA NPs groups displayed upped levels compared with that of OXA groups, especially LY and PLT (***Figure 5***(A–G)). In addition, hepatotoxicity and nephrotoxicity were evaluated by monitoring TP, ALB, UREA and Cr in plasma taken from treated mice. No significant change in biochemical indexes was found from mice treated with OXA except of the significant decrease of UREA in OXA (10 mg/kg) group. On the contrary, all PEG-OXA NPs groups could cause a significant increase in ALP and TP (Figure 4(D–G)). In conclusion, these results revealed that PEG-OXA NPs strategy was able to cause remarkably less systemic toxicity than the clinically used OXA and promote the tolerability of chemotherapy. The relative body weight change in antitumor activity study could also confirm this observation (***Figure 6***(C)).

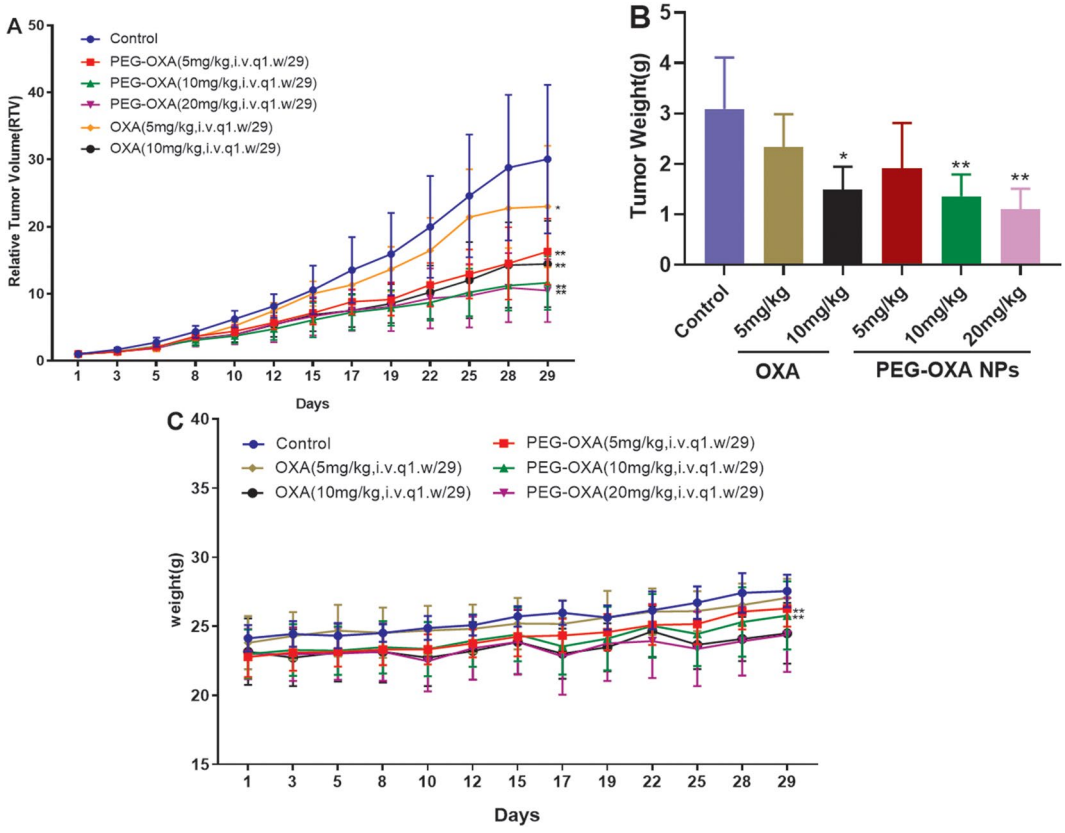

Figure 6. Antitumor efficacy of PEG-OXA NPs. (A) Tumor growth profiles of mice receiving OXA (5 and 10 mg/kg) or PEG-OXA NPs (5, 10 and 20 mg/kg in OXA). (B) Weights of tumors collected from mice at the end of the efficacy experiment. (C) Bodyweight changes of mice receiving OXA (5 and 10 mg/kg) or PEG-OXA NPs (5, 10 and 20 mg/kg in OXA). All data were presented as mean ± SD ($n = 6$). *$p < .05$, **$p < .01$.

3.6. In vivo antitumor activity

The in vivo antitumor activity of PEG-OXA NPs was also assessed in SW260 xenograft tumor-bearing mice. OXA was administrated at 5 mg/kg and 10 mg/kg, while PEG-OXA NPs were given at three different dosages (5, 10 and 20 mg/kg in OXA) at 0, 7, 14, 21 and 28 days after treatment initiation. Figure 6(A–C) demonstrated the tumor volume and body weight change in different drug-treated mice. The results revealed that a dose-dependent tumor growth inhibition was observed both in PEG-OXA NPs and OXA solution groups (Figure 6(A)). PEG-OXA (10 mg/kg and 20 mg/kg in OXA) dramatically inhibited the tumor growth compared with control ($P < 0.01$). The tumor volume and tumor weight of PEG-OXA were significantly lower than those of OXA equivalent. The improved efficacy of PEG-OXA NPs than OXA might be mainly a result of prolonged and elevated free drug exposure in the tumor.

4. Conclusions

In this research, we designed a Pt(IV) prodrug (PEG-OXA) that could self-assemble into nanoparticles for self-delivery of OXA. PEG-OXA NPs had small particle size and the low CMC value that maintained the nanoparticles stable in blood circulation system. The release of OXA from PEG-OXA NPs showed the characteristic of responding to release in a reducing environment. PEG-OXA NPs displayed longer blood circulation duration while lower OXA concentrations in plasma than that of OXA solution. PEG-OXA NPs exhibited satisfactory antitumor activity and low systemic toxicity. These results demonstrated that the reduction-responsive Pt(IV) prodrug NPs might be a desirable strategy for improving the therapeutic activity of current platinum drugs.

Disclosure statement

There are no conflicts to declare.

Author contributions

Yuanlei Fu, Qiuyan Zhang and Rong Rong designed and conducted the experiments. Yuanlei Fu, Dongfang Cheng and Yuqian Hou synthesized and prepared the compounds. Ying Kong analyzed the data and wrote the article. Yan Li, Tongfang Li, Yani Xiao, and Xiangping Li performed experiments. Qiuyan Zhang and Rong Rong reviewed and edited the article.

Funding

This work was supported by National Natural Science Foundation of China (Grant No. 82204497).

References

Ding F, Zhang LP, Chen H, et al. (2020). Enhancing chemotherapy efficacy of platium prodrug nanoparticles and inhibiting cancer metastasis via targeting iron homeostasis. Nanoscale Horiz 5:1–10.

Feng B, Zhou FY, Hou B, et al. (2018). Binary cooperative prodrug nanoparticles improve immunotherapy by synergistically modulating immune tumor microenvironment. Adv Mater 30: e1803001.

Gibson D. (2016). Platinum(IV) anticancer prodrugs-hypotheses and facts. Dalton Trans 45:12983–91.

He L, Sun M, Cheng X, et al. (2019). H/Redox dual-sensitive platinum(IV)-based micelles with greatly enhanced antitumor effect for combination chemotherapy. J Colloid Interf Sci 541:30–41.

Ho GY, Woodward N, Coward JI. (2016). Cisplatin versus carboplatin: comparative review of therapeutic management in solid malignancies. Crit Rev Oncol Hematol 102:37–46.

Huang J, Ding W, Zhu X, et al. (2022). Ligand evolution in the photoactivatable platinum(IV) anticancer prodrugs. Front Chem 10:876410.

Ibrahim A, Hirschfeld S, Cohen MH, et al. (2004). FDA drug approval summaries: oxaliplatin. Oncologist 9:8–12.

Ito H, Yamaguchi H, Fujikawa A, et al. (2012). A full validated hydrophilic interaction liquid chromatography-tandem mass spectrometric method for the quantifification of oxaliplatin in human plasma ultrafiltrates. J Pharmaceut Biomed 71:99–103.

Johnstone TC, Suntharalingam K, Lippard SJ. (2016). The next generation of platinum drugs: targeted Pt(II) agents, nanoparticle delivery, and Pt(IV) prodrugs. Chem Rev 116:3436–86.

Kelland L. (2007). The resurgence of platinum-based cancer chemotherapy. Nat Rev Cancer 7:573–84.

Kenny RG, Chuah SW, Crawford A, et al. (2017). Platinum (IV) prodrugs: a step closer to Ehrlich's vision? Eur J Inorg Chem 2017:1596–612.

Khor SY, Hu J, McLeod VM, et al. (2016). The pharmacokinetics and biodistribution of a 64 kDa PolyPEG star polymer after subcutaneous and pulmonary administration to rats. J Pharm Sci 105:293–300.

Lang TT, Li NN, Zhang J, et al. (2021). Prodrug-based nano-delivery strategy to improve the antitumor ability of carboplatin in vivo and in vitro. Drug Deliv 28:1272–80.

Ling X, Chen X, Riddell IA, et al. (2018). Glutathione-scavenging poly(disulfide amide) nanoparticles for the effective delivery of Pt(IV) prodrugs and reversal of cisplatin resistance. Nano Lett 18:4618–25.

Miller MA, Zheng YR, Gadde S, et al. (2015). Tumour-associated macrophages act as a slow-release reservoir of nano-therapeutic Pt(IV) pro-drug. Nat Commun 6:8692.

Motzer RJ, Mazumdar M, Gulati SC, et al. (1993). Phase-II trial of high-dose carboplatin and etoposide with autologous bone-marrow transplantation in 1st-line therapy for patients with poor-risk germ-cell tumors. J Natl Cancer Inst 85:1828–35.

Oun R, Moussa YE, Wheate NJ. (2018). The side effects of platinum-based chemotherapy drugs: a review for chemists. Dalton Trans 47:6645–53.

Pasut G, Veronese FM. (2009). PEG conjugates in clinical development or use as anticancer agents: an overview. Adv Drug Deliv Rev 61:1177–88.

Rudmann DG, Alston JT, Hanson JC, et al. (2013). High molecular weight polyethylene glycol cellular distribution and PEG-associated cytoplasmic vacuolation is molecular weight dependent and does not require conjugation to proteins. Toxicol Pathol 41:970–83.

Song XQ, Liu RP, Wang SQ, et al. (2020). Anticancer melatplatin prodrugs: high effect and low toxicity, MT1-ER-target and immune response in vivo. J Med Chem 63:6096–106.

Song XQ, Ma ZY, Wu YG, et al. (2019). New NSAID-Pt(IV) prodrugs to suppress metastasis and invasion of tumor cells and enhance anti-tumor effect in vitro and in vivo. Eur J Med Chem 167:377–87.

Wang Q, Xiao M, Wang DY, et al. (2021). In situ supramolecular self-assembly of Pt(IV) prodrug to conquer cisplatin resistance. Adv Funct Mater 31:2101826.

Wang L, Huang J, Chen H, et al. (2017). Exerting enhanced permeability and retention effect driven delivery by ultrafine iron oxide nanoparticles with T(1)-T(2) switchable magnetic resonance imaging contrast. ACS Nano 11:4582–92.

Wang XH, Li M, Ren KB, et al. (2020). On-demand autophagy cascade amplification nanoparticles precisely enhanced oxaliplatin-induced cancer immunotherapy. Adv Mater 32:2002160.

Wang ZG, Kuang GZ, Yu ZQ, et al. (2019). Light-activatable dual prodrug polymer nanoparticle for precise synergistic chemotherapy guided by drug-mediated computed tomography imaging. Acta Biomater 94:459–68.

Xiao HH, Noble GT, Stefanick JF, et al. (2014). Photosensitive Pt(IV)–azide prodrug-loaded nanoparticles exhibit controlled drug release and enhanced effifficacy in vivo. J Control Release 173:11–17.

Xu C, Wang Y, Guo Z, et al. (2019). Pulmonary delivery by exploiting doxorubicin and cisplatin co-loaded nanoparticles for metastatic lung cancer therapy. J Control Release 295:153–63.

Xu ZW, Li QD, Zhang C, et al. (2022). Amorphous ferric oxide-coating selenium core–shell nanoparticles: a self-preservation Pt(IV) platform for multi-modal cancer therapies through hydrogen peroxide depletion-mediated anti-angiogenesis, apoptosis and ferroptosis. Nanoscale 14:11600–11.

Yao HZ, Xu ZF, Li C, et al. (2019). Synthesis and cytotoxic study of a platinum(IV) anticancer prodrug with selectivity toward luteinizing hormone-releasing hormone (LHRH) receptor-positive cancer cells. Inorg Chem 58:11076–84.

Zhang LW, Qian M, Cui HY, et al. (2021). Spatiotemporal concurrent liberation of cytotoxins from dualprodrug nanomedicine for synergistic antitumor therapy. ACS Appl Mater Interfaces 13:6053–68.